Publications of the Astronomical Society of the Pacific, **119**: 1114–1125, 2007 October

A Closed Loop Layer-oriented Adaptive Optics Test Bed: Applications to Ground-Layer Adaptive Optics

S. E. Egner, W. Gaessler, and T. M. Herbst

Max Planck Institute for Astronomy, Heidelberg, Germany; egner@mpia.de

and

R. Ragazzoni

Osservatorio Astronomico di Padova, Padova, Italy

Received 2007 April 27; accepted 2007 August 8; published 2007 October 25

ABSTRACT. Turbulence in Earth's atmosphere severely limits the achievable image quality of ground-based optical telescopes. With the technique of adaptive optics, the induced distortions of the light can be measured and corrected in real time, regaining nearly diffraction limited performance. Unfortunately, when using a single guide star to measure the distortions, the correction is only useful within a small angular area with a radius of ∼3″ centered on the guide star. This paper presents a laboratory setup, using four simulated natural guide stars and one deformable mirror to measure and correct turbulence-induced distortions over ∼35″ × 22″. With such a layer-oriented ground-layer adaptive optics (GLAO) system, the area of useful correction is significantly increased. We characterize a test bed for such a system in static and dynamic operation and verify the principles of the layer-oriented technique in closed loop operation. Furthermore, we study the influence of nonconjugated turbulent layers and the effect of brightness variations of the guide stars and derive results very similar to theoretical predictions and numerical simulations.

Online material: color figures

1. INTRODUCTION

Spatial and temporal variations in the index of refraction in Earth's atmosphere induce a shift in the phase of individual light rays. This results in a deformation of the imaginary surface of constant phase in a parallel beam of light, also called the wave front. When a star is observed with a telescope, the distorted wave front causes the stellar image to be decomposed into many small so-called speckles. For integration times longer than a few tens of milliseconds, the motion of the speckles smears the stellar image to the seeing disk, which has a diameter of typically 1″ in the visible and thus is several orders of magnitude worse than the diffraction limit. The technique of adaptive optics (AO) was proposed in the 1950s (Babcock 1953) to correct for the effects of this turbulence and to regain nearly diffraction limited image quality. However, it was not until the early 1990s that the technological challenges could be solved to apply this method to astronomical observations. Due to the scientific success of the technique, today AO instruments are in operation at almost all large ground-based telescopes.

Classical AO systems use one natural guide star to measure the deformations of the incoming wave front with a wave front sensor (WFS) and to correct them with a deformable mirror (DM). However, since light originating from objects other than the guide star experiences different deformations by the turbulent atmosphere, the correction by such an AO system degrades rapidly with the distance from the guide star. The isoplanatic angle is a measure of the maximum angular separation from the guide star with still acceptable correction, which is typically 20″ in K band and 3″ in the visible. To increase ϑ_0 and thus the area of homogenous correction, the concept of multiconjugate adaptive optics (MCAO) was proposed (Beckers 1988; Rigaut et al. 2000). Several guide stars are used in this technique to measure the vertical structure of the turbulence in the complete volume above the telescope. Several DMs are placed optically at the altitudes of the most turbulent layers, thus compensating the turbulence in individual layers rather than for a single direction. The result is that the maximum achievable performance on-axis is not as good as with classical AO, because of uncorrected turbulence between the single corrected layers, but that the correction is much more uniform over a significantly increased field of view (FOV).

Measurements of the vertical distribution of the atmospheric turbulence at various sites show that the optically active turbulence is strongly concentrated near the ground (see, e.g., scintillation detection and ranging [SCIDAR] measurements at San Pedro Martir [Avila et al. 2004], Mt. Graham [Egner et al. 2006], Pic du Midi [Prieur et al. 2001], and Mauna Kea [Racine & Ellerbroek 1995]). Typically 60%–75% of the total atmospheric turbulence is within the first 2 km above the

ground. A significant improvement of the image quality can therefore already be achieved by correcting just the turbulence near the ground. Rigaut (2002) thus proposed a "MCAO-light" system, i.e., to measure and correct only the ground-layer turbulence. This technique is now called ground-layer adaptive optics (GLAO). There are two possibilities to separate the wave front aberrations introduced by the ground layer from the other, higher altitude turbulent layers. The first possibility is to use a single artificial guide star, created with a laser beacon at an altitude of a few kilometers above the telescope, and thus sample only the turbulence below the altitude of this laser guide star (LGS). This approach is currently being pursued by a number of observatories (e.g., for Giant Magellan Telescope [Athey et al. 2004], European Southern Observatory [ESO; Hubin et al. 2004], William Herschel Telescope [Morris et al. 2004], and Southern Astrophysical Research [SOAR; Tokovinin et al. 2004]).

The other option is to use more than one guide star and then—as with a full-fledged MCAO system—to retrieve the wave front aberrations introduced by the single layers from the correlation of the wave front aberrations in different directions. An elegant implementation of this method can be accomplished with a pupil plane wave front sensor (e.g., a pyramid as proposed by Ragazzoni 1996) and the layer-oriented technique (Ragazzoni et al. 2000; Farinato et al. 2004a), where the discrimination of the contribution of individual layers to the total wave front deformation is done optically.

Simulations of GLAO systems predict a relatively low Strehl ratio, but a significantly reduced FWHM of the PSF over a rather wide FOV (Rigaut 2002; Arcidiacono 2004; Tokovinin 2004; Nicolle et al. 2004; Andersen et al. 2006; Le Louarn & Hubin 2006). Such a GLAO system would be well suited for scientific applications, such as spectroscopy, where a diffraction-limited image is not required, but a significant gain is already achieved for an effective reduction of the seeing by a factor of ~2.

Open loop measurements with a Shack-Hartmann wave front sensor and four guide stars have already demonstrated the GLAO principle (Baranec et al. 2003, 2007). However, up to now, no layer-oriented GLAO or MCAO system using several natural guide stars is running in closed loop on the sky. To verify the concepts and to gain valuable experience with the alignment, operation, and control of a GLAO system, we set up a laboratory experiment, including all the relevant components (dynamic atmosphere simulator, deformable mirror, layer-oriented wave front sensor unit, and control software). Operating this system in closed loop, we can study the layer-oriented principle with optical co-addition for the first time in detail under realistic atmospheric conditions. This paper presents the results of these extensive tests.

After this introductory section, the system is described in detail in § 2. In § 3 the main results obtained in ground-layer AO mode are presented and compared to single-star AO mode. A summary in § 4 concludes this paper.

2. SYSTEM DESCRIPTION

Figures 1 and 2 show the complete setup with the individual components. This section provides some details on the individual system components.

2.1. The Light Source

To simulate the guide stars, we used a metal plate with small holes as a mask in front of a halogen lamp. The mask contains four guide star holes located at the corners of a rectangle with dimensions ~35″ × 22″. The diameters of the holes correspond roughly to the size of the seeing disk in order to simulate a modulation of the pyramids (Costa 2005) and therefore to allow adjustment of the linear range of the pyramid to the amplitude of the wave front aberrations induced by the turbulence simulator. A single mode fiber is attached to a central hole in the metal plate and illuminated by a laser with $\lambda = 835$ nm. This fiber, subsequently referred to as the science fiber, has a core diameter of ~5 μm and serves as a diffraction-limited reference for independently and unambiguously determining the loop performance.

2.2. Dynamic Turbulence Simulator

In order to dynamically test next-generation AO systems for Calar Alto, the Very Large Telescope (VLT), and the Large Binocular Telescope, a dedicated atmospheric turbulence simulator was developed and built at the Max Planck Institute for Astronomy (MPIA) over the last few years (Butler et al. 2004; Hippler et al. 2006a, 2006b). This multiple atmospheric phase screens and stars (MAPS) system consists of a collimator, a reimager. and several rotating phase screens. The symmetric optical design was optimized to simulate the focal plane of the VLT (8 m telescope, f/15, and same curvature of the focal plane) and to deliver diffraction-limited performance in the wavelength range from 0.5 to 2.2 μm over the complete 2′ FOV.

Rotating, etched glass plates, manufactured by Silios, with a diameter of 10 cm were used to simulate the atmospheric turbulence. Up to three such phase screens with various numbers of etching steps can be inserted in MAPS, resulting in a simulated seeing between 0.3″ and 1.5″ in the visible. The altitude of the phase screens can be adjusted continuously between 100 m and 15 km above the telescope, and the temporal evolution of the turbulence can be adjusted with the rotation speed of the motors.

2.3. The Telescope Simulator

After the light passes the turbulence simulator, it is collimated to form an image of the pupil on the DM and then refocused to feed the WFS unit. The collimating and refocusing arm each consist of three lenses, delivering a diffraction-limited image over the complete FOV for monochromatic light. Even for white light, the shift of the pupil images on the WFS CCD

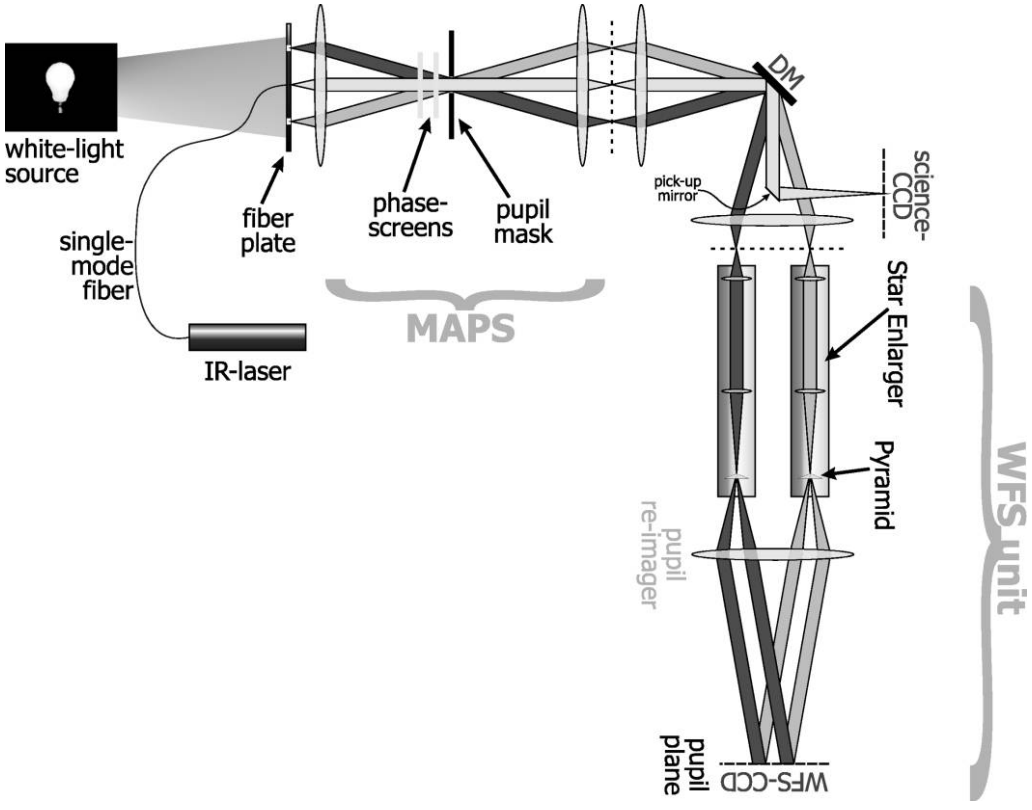

FIG. 1.—Schematic diagram of the complete lab setup. The relative sizes and angles are not to scale. The guide stars are simulated by a metal plate with small holes, which we illuminated from the back by a white-light source. A single-mode fiber is also glued into this metal plate. This fiber is attached to an infrared laser and is used to simulate a diffraction-limited science object. Inside the turbulence simulator "MAPS," the light is first collimated, passes several phase screens to induce wave front aberrations, and is finally focused again. Another collimator images the pupil onto the deformable mirror, and the reflected light is focused by another set of optics. The light of the science object is reflected by a small pickup mirror into the science camera, while the light of the guide stars enters the wave front sensor unit. The focal ratio on the tip of the pyramid is increased individually for each guide star with the help of two lenses. These are mounted together with the pyramid on a "star enlarger" to move them to the position of the guide star in the field while keeping their mutual alignment. In this lab setup, a total of four pyramids is used. For reasons of clarity only two are shown here. A common lens reimages the pupils of all four pyramids on the wave front sensor CCD. In GLAO mode, the focus of this lens is adjusted to achieve perfect overlap of the pupil images of all four pyramids on the WFS-CCD. [*See the electronic edition of PASP for a color version of this figure.*]

for different wavelengths is only 0.625% of the pupil diameter. For 30 × 30 subapertures, this chromatic smearing is less than 0.2 subapertures and thus does not affect the achievable performance of this system (Diolaiti et al. 2005). However, the use of commercially and readily available lenses limits the diameter of the pupil image on the DM to 65 mm, resulting in 10 × 10 actuators across the pupil.

2.4. The Deformable Mirror

We used a continuous face-sheet DM with 349 piezo actuators by Xinetics, Inc., to correct the wave front aberrations induced by MAPS. To guarantee optimal control and representation of Zernike modes, the DM and its electronics were extensively characterized (Egner et al. 2004; Stuik et al. 2004) for such parameters as the surface flatness, linearity, hysteresis, gain, and influence functions of all the actuators. Together with the determination of the required voltages to get an optically flat mirror surface, the DM can routinely be controlled at room temperature to an accuracy of ~20 nm rms between 0 and 75% of the full stroke of 6 μm.

2.5. Wave Front Sensor Unit

The core of the lab setup is the wave front sensor. This unit implements the concept of a layer-oriented GLAO system with optical co-addition by using four pyramids to measure the wave front aberrations of four natural guide stars (Ragazzoni et al. 2002; Farinato et al. 2004b). In the case of a pyramid wave front sensor, the wave front camera is focused to the desired conjugation altitude and the pupil images of the single pyramids overlap on the detector according to their footprint at the conjugation altitude (see Fig. 3).

To achieve a reasonable linear range, the size of the Airy disk has to be larger than the size of the tip of the pyramid (Costa 2005). Rounded edges on the order of ~10 μm thus require an ~f/200 beam for a wavelength of 0.5 μm at an 8 m telescope. However, for a layer-oriented MCAO system, this

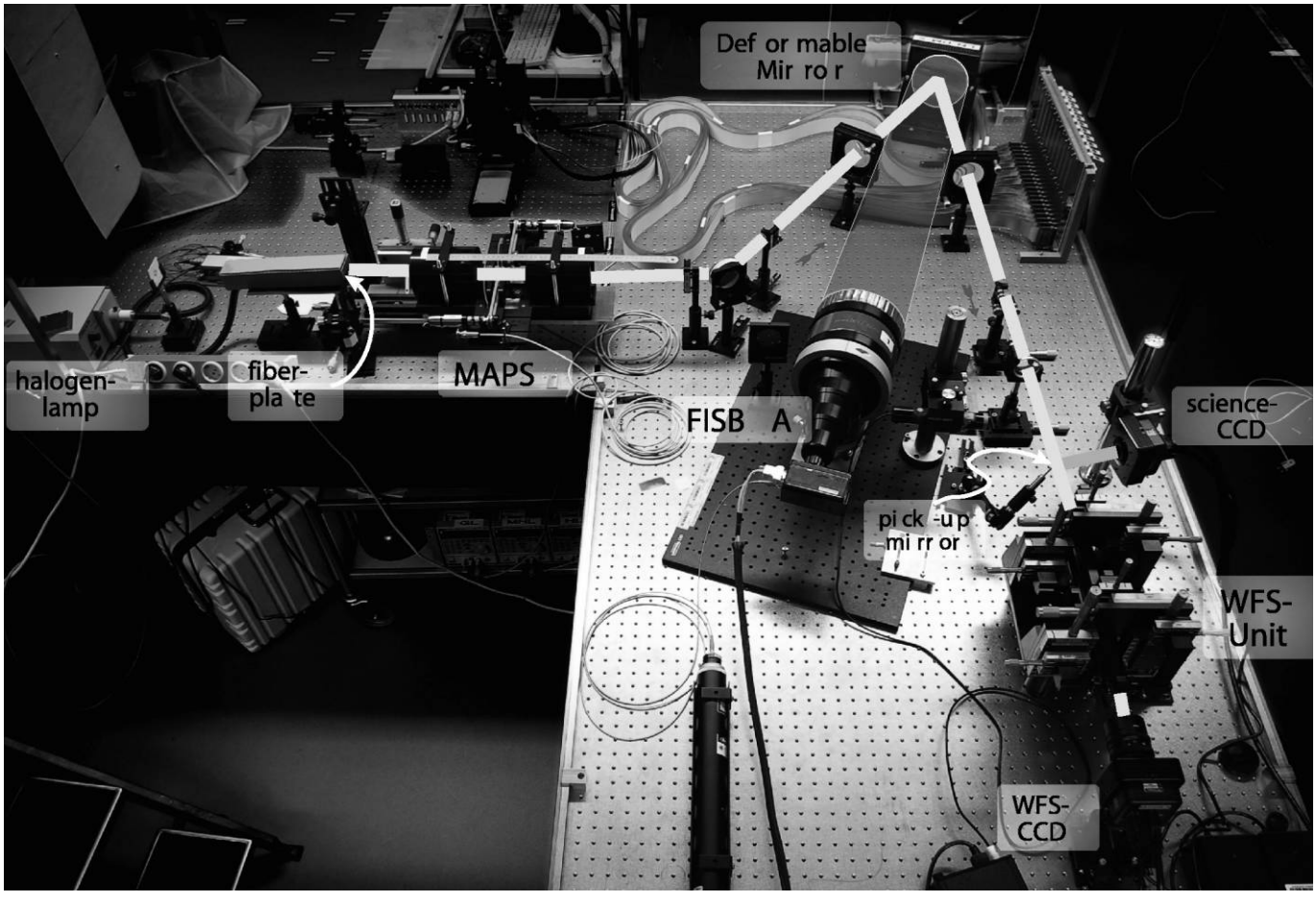

FIG. 2.—Photo showing the complete lab setup with the light source (halogen lamp and fiber plate), the turbulence generator (MAPS), collimating optics, deformable mirror, refocusing optics, science camera, and wave front sensor unit. The FISBA interferometer is used for monitoring and calibration of the DM. The light path is indicated by the thick gray line. [*See the electronic edition of PASP for a color version of this figure.*]

cannot be achieved by increasing the f-ratio of the complete beam because the diameter of the focal plane would increase by the same factor, requiring huge lenses to image the pupils onto the WFS-CCD. For a 2′ FOV at a modern 8 m, f/15 telescope, this would require a focal plane and thus a pupil reimaging lens of more than 1 m diameter, which is economically not feasible.

A possible solution is to enlarge the f-ratio *locally* (Ragazzoni et al. 2005). This can be achieved with so-called star enlargers, as shown in Figure 1. Each star enlarger contains two lenses and one pyramid. The first lens with a short focal length f_1 collimates the light, while the second lens with a longer focal length f_2 focuses the light onto the tip of the pyramid. Each star enlarger is mounted on a stage to allow positioning and tilt for optimal overlap of the pupil images of the single pyramids on the WFS-CCD. The pyramids were manufactured by grinding commercial flat-convex BK7 lenses to a vertex angle of 1.0°.

Finally, a common lens with a focal length $f = 75$ mm images the pupils onto the WFS-CCD (Fig. 3). By adjusting the focus of this lens, the detector can be easily conjugated to different altitudes without having to change the complete setup. We used a DVC-1412 frame-transfer camera with a Camera Link interface. This camera has a frame rate of up to 60 Hz for the used size of the interesting subarray with the pupil images. This rather low frame rate is not problematic because by adjusting the rotation speed of the phase screens, any ratio between the wind speed v_w and thus the timescale of the turbulence evolution and the frame rate $f_{\rm loop}$ of the AO system can be emulated. For the experiments described in this paper, we used a corresponding $f_{\rm loop}/v_w$ between 5 and 25 $\rm m^{-1}$.

3. GROUND-LAYER AO MEASUREMENTS

3.1. Filtering of Nonconjugated Heights

An analytic theory to describe how well single turbulent layers can be seen and thus corrected with an MCAO system was presented by, e.g., Tokovinin et al. (2000), Owner-Petersen & Gontcharov (2002), and Jolissaint et al. (2004). To test this theory experimentally and verify the layer-oriented principle,

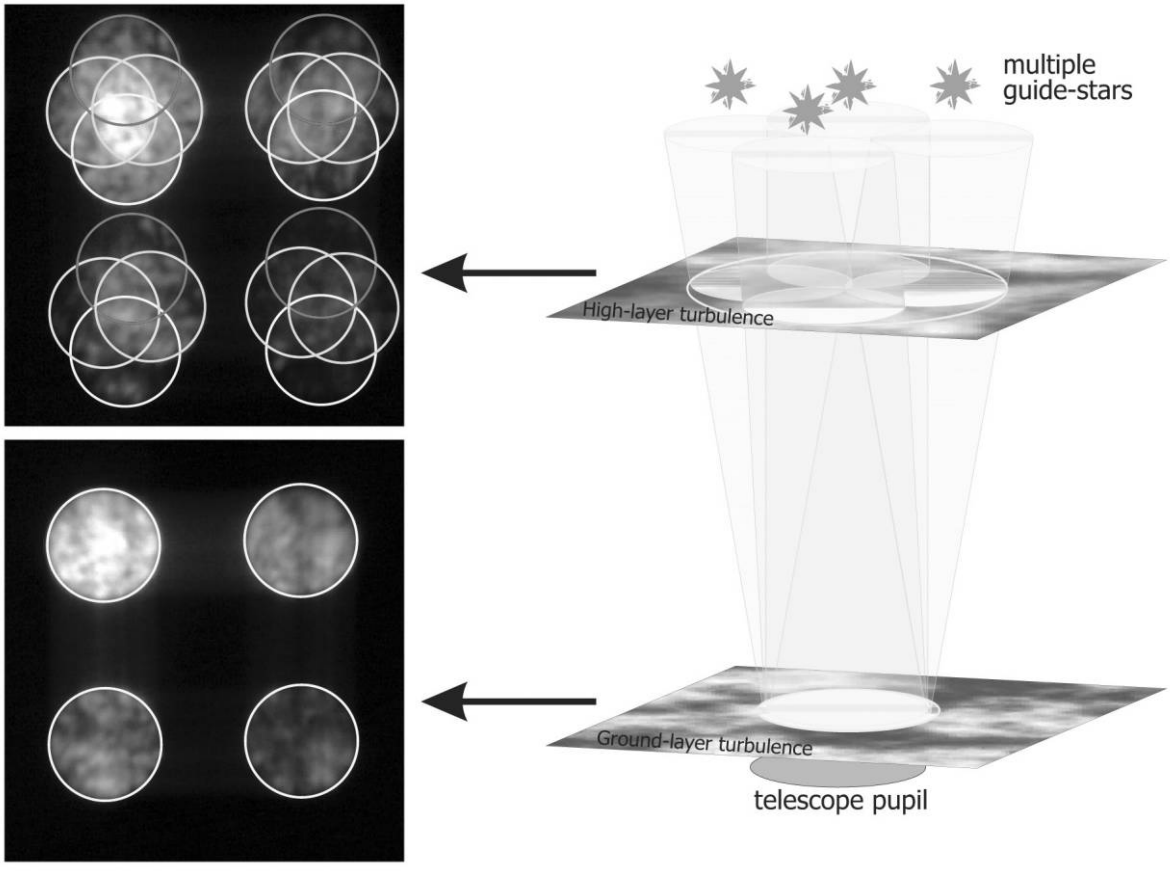

FIG. 3.—Examples of the pupil images produced by the four pyramids in the presence of turbulence, measured with the WFS unit of the presented lab setup when the detector is conjugated to the ground (*bottom left*) and to a high layer (*top left*). When conjugated to the ground, the pupil images of all guide stars overlap perfectly. In contrast, the pupil footprints on the turbulent layer and thus on the CCD are shifted according to the positions of the stars in the field for high-layer conjugation, as indicated by the different colors of the overplotted circles. [*See the electronic edition of PASP for a color version of this figure.*]

we varied the conjugation height of the phase screens in MAPS, while the WFS-DM combination was kept conjugate to the pupil plane. The performance in closed loop was then measured for various positions of the phase screens.

Figure 4 shows the Strehl ratio and the FWHM of the PSF in GLAO mode as a function of the altitude of the turbulent layer. Also shown for comparison is the performance in single-star mode. We used the measured values of the FWHM for comparison to theoretical predictions because, for values below ~15%, the Strehl ratio is not a simple function of the variance of the wave front but instead critically depends on the precise but unknown structure of the aberrations. In these low-Strehl conditions, the FWHM is less sensitive to such effects and is therefore a better measure of the performance.

The theoretical value for the FWHM can be calculated from the variance of the wave front aberrations $\sigma^2_{\rm sci}$, which is related to the Fried parameter r_0 by (Noll 1976)

$$\sigma^2_{\rm sci} = 1.030\left(\frac{D}{r_0}\right)^{5/3}, \tag{1}$$

which in turn can be used to calculate the FWHM via (Fried 1965)

$$\mathrm{FWHM} = 0.98\,\frac{\lambda}{r_0}. \tag{2}$$

3.1.1. Single-Star Adaptive Optics

For single-star AO, $\sigma^2_{\rm sci}$ was calculated from the overlap of the pupil footprints on the turbulent layer (Fig. 5). The total wave front variance $\sigma^2_{\rm sci}$ can be divided into two contributions. In the area $A_C(h,\alpha)$ of the pupil footprint of the science object, which overlaps with the pupil footprints of the guide stars, the

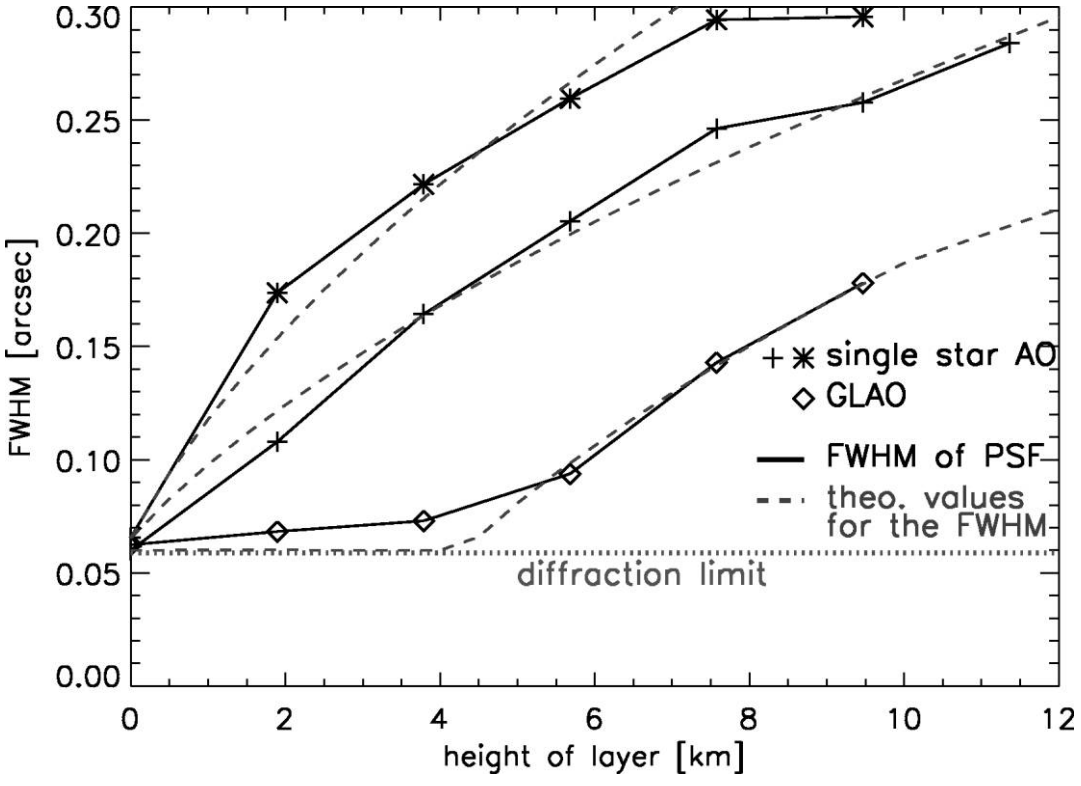

FIG. 4.—FWHM of the PSF in closed loop as a function of the height of the phase screen above the pupil plane in GLAO operation. For comparison, the performance of a single-star AO system with the science object at 14″ and 17″ distance from the guide star is shown. The theoretical values are calculated as explained in the text. [*See the electronic edition of PASP for a color version of this figure.*]

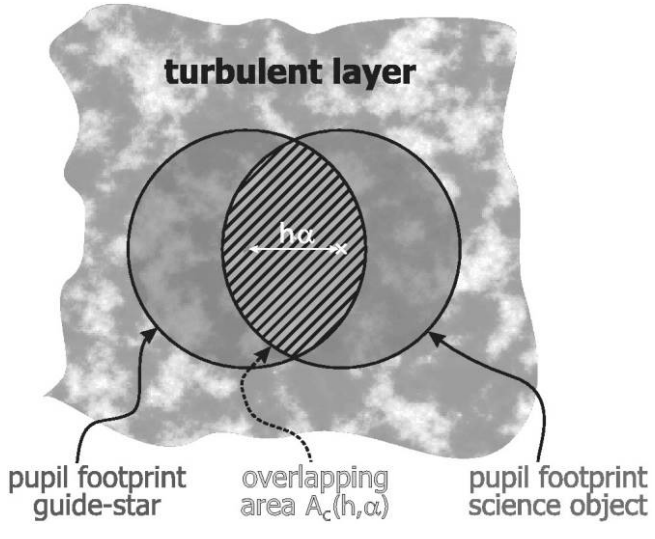

FIG. 5.—Overlap region on a turbulent layer for the pupil footprints of the guide star and the science object for a classical AO system with one guide star and one single turbulent layer. [*See the electronic edition of PASP for a color version of this figure.*]

wave front aberrations can be measured and corrected with the AO system and thus contribute with a residual variance $\sigma^2_{\rm cl}$. In the rest of the pupil footprint of the science object, the aberrations with a variance $\sigma^2_{\rm layer}$ are those of the uncorrected atmosphere and are known from the open loop performance. For the science object, the total residual wave front aberrations $\sigma^2_{\rm sci}$ are therefore given as a sum of $\sigma^2_{\rm cl}$ and $\sigma^2_{\rm layer}$, weighted with their respective areas in the science object pupil footprint on the turbulent layer:

$$\sigma^2_{\rm sci}(h,\alpha) = \left[\frac{A_C(h,\alpha)}{A_{\rm tel}}\right]\sigma^2_{\rm cl} + \left[\frac{A_{\rm tel} - A_C(h,\alpha)}{A_{\rm tel}}\right]\sigma^2_{\rm layer}. \qquad (3)$$

Here $A_{\rm tel} = D^2_{\rm tel}(\pi/4)$ is the size of the individual pupil footprints on the layer; $A_C(h,\alpha)$ can be calculated analytically as a function of the altitude h of the turbulent layer and the angular separation α between the guide star and the science object. As shown in Figure 4, for one turbulent layer, this model nicely fits the measurements.

3.1.2. Ground-Layer Adaptive Optics

For the GLAO mode, the theoretical performance expectations were determined with the help of layer filter functions

for this system, as defined in Tokovinin et al. (2000), Owner-Petersen & Gontcharov (2002), and Jolissaint et al. (2004) and shown in Figure 6. These functions describe which fraction of the wave front variance can be seen with a layer-oriented WFS and then also be corrected by a given number of Zernike modes on the DM. Multiplying the wave front variance σ^2_{layer}, as determined from open loop measurements, by the corresponding value of the layer filter function at the given altitude h gives the expected FWHM of the PSF via equations (1) and (2). Figure 4 shows that all measurements very nicely follow the theoretical predictions.

The fact that the FWHM in GLAO operation is constant if the altitude of the turbulent layer is less than ~4 km can be explained with the help of the layer filter functions. For a given number of reconstructed modes, the correction by the AO system is effective only up to a certain spatial frequency. When moving the turbulent layer away from the conjugation plane of the WFS, the uncorrected high spatial frequencies are smeared out first, while the corrected, lower spatial frequencies and, thus, the closed loop performance are barely influenced. As noted by Tokovinin (2004) all turbulent layers below a certain altitude H_{min} (~4 km in this case) are thus equally well corrected; the correction depends only on the parameters of the AO system, such as the actuator spacing and the FOV.

When moving the turbulent layer to higher altitudes, the—in principle—correctable low spatial frequencies are also affected by the smearing; the image quality thus starts to deteriorate. For a certain desired FWHM and FOV of the system, there is thus a maximal altitude H_{max} of the turbulent layers, below which the turbulence can still be sufficiently well corrected to achieve this performance. The region between H_{min} and H_{max} is also called the "gray zone" because turbulence in this altitude range is critical for the performance of the system (Tokovinin 2004). The theoretical value is $H_{\text{max}} \sim \lambda/(\text{FWHM} \times \text{FOV})$, with the observing wavelength λ, the desired FWHM, and the given FOV of the system. Using, for example, FWHM ~ 0.15″, the theoretical value for our system for $H_{\text{max}} \sim 7900$ m fits very nicely with the measurements (Fig. 4).

3.2. Modal Covariance Matrix

A good measure to describe this filtering effect of nonconjugated turbulent layers as a function of spatial frequency is the Zernike modal covariance matrix (Noll 1976). Since Zernike modes are approximately sorted by spatial frequency, the temporal averaged variances of the individual modal coefficients correlate with the spatial power spectral density of the wave front aberrations.

The Zernike modal covariance matrix was measured for various distances between the conjugation altitudes of the turbulent layer and the WFS. The result, plotted in Figure 7, clearly shows the increase of the filtering effect for increasing distance of the turbulent layer from the conjugation plane of the WFS. The open loop data also show that the filtering effect is more pronounced for high-order modes. However, the overall filtering is not as strong as expected from theoretical predictions. The reason is that an infinite number of guide stars was assumed in the theoretical calculations, which might not be a good approximation for the case of only four guide stars. For only four guide stars, the small number of overlapping pupils with slightly shifted positions is not sufficient to homogeneously smear out all spatial frequencies.

As seen in the previous section and Figure 4, the adaptation of the conjugation heights of the DMs to the vertical structure of the atmospheric turbulence is crucial to achieve optimal performance of an MCAO system. Since simultaneous SCIDAR measurements, for example, are not feasible for all MCAO observations, information about the vertical structure of the atmospheric turbulence has to be retrieved by different means. One idea is to use the measured modal covariance matrix of the high-layer DM. For maximum Strehl ratio on-axis, this DM has to be conjugated to the strongest turbulent layer in the free atmosphere. If all layers obey the Kolmogorov model, then the high-layer DM has to be placed at the altitude where the ratio of the temporal averaged variances of the high- to low-order modal coefficients is maximum. For a misconjugation, the high spatial frequencies are attenuated with respect to the low spatial frequencies, decreasing this ratio.

Figure 7 suggests that the determination of the optimal conjugated height from the measured modal variances is possible, with a vertical resolution of a few kilometers. However, it is doubtful whether this vertical resolution is sufficient for this application (Fig. 4). However, as explained above, for more guide stars and a larger FOV, the filtering effect should be more pronounced, making the distinction of closely separated layers easier and thus increasing the vertical resolution.

3.3. Off-Axis PSF Structure

One of the main advantages of a GLAO system is that the shape of the PSF is supposed to be more uniform over the FOV, compared to single-star AO (Rigaut 2002; Arcidiacono 2004; Tokovinin 2004; Jolissaint et al. 2004; Andersen et al. 2006; Le Louarn & Hubin 2006). We mounted the science fiber at various off-axis positions in order to measure the shape of the PSF in closed loop at different positions in the field. Due to optomechanical constraints, only three guide stars could be used for these measurements.

As shown in Figure 8, in GLAO mode and for one turbulent layer at 5.6 km above the pupil plane, the FHWM is less than twice the diffraction limit over a field with 30″ diameter. This is a dramatic improvement in performance compared to single-star AO, where the FWHM increases almost exponentially with distance to the guide star. For single-star AO, the FWHM is already more than twice the diffraction limit at a distance of 3″ from the guide star. The area of useful correction is thus increased in GLAO mode by a factor of ~25. This confirms

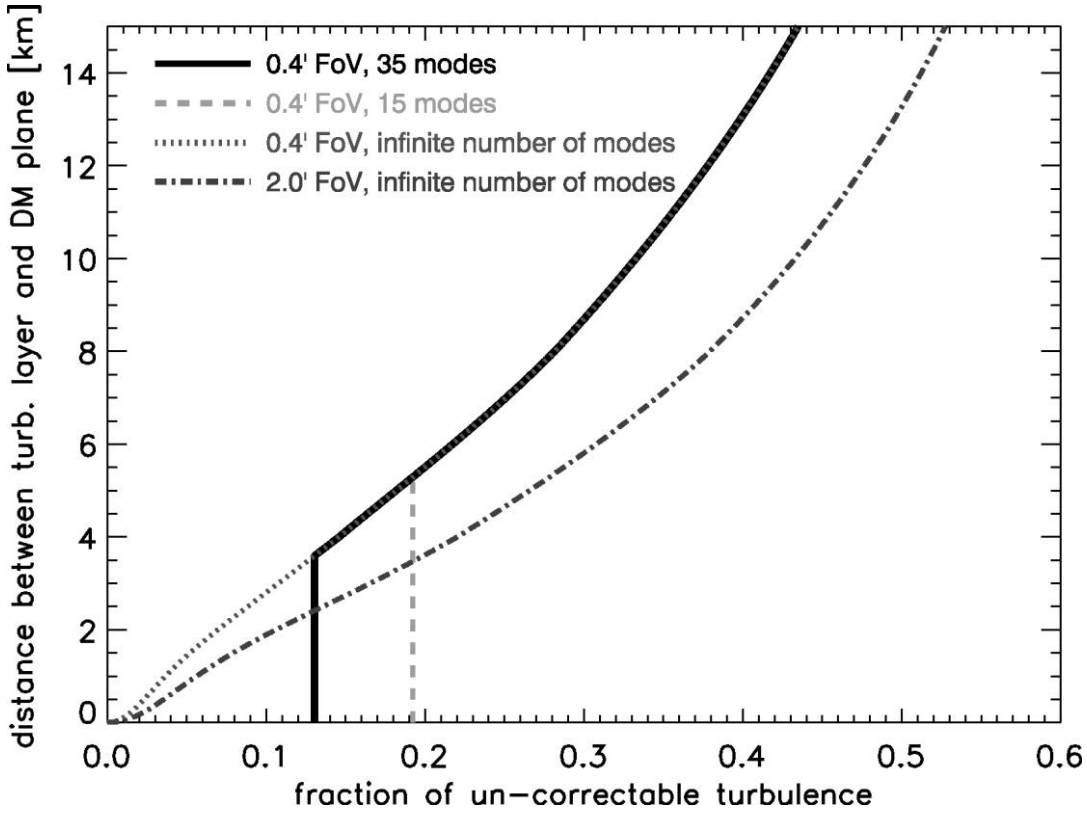

FIG. 6.—Layer filter functions for different numbers of corrected modes and sizes of the FOV of a layer-oriented WFS. Close to the WFS/DM plane most of the turbulence is seen and can be corrected. For example, only 1.7% (0.13^2) of the wave front variance remains uncorrected in the first 4 km above the ground for 35 corrected Zernike modes and 0.4′ WFS-FOV. These remaining wave front aberrations are either not seen by the WFS because they are defocused, or they consist of too-high spatial frequencies, which cannot be compensated with the limited number of modes corrected by the DM. [*See the electronic edition of PASP for a color version of this figure.*]

the notion that homogenous performance can be achieved over the entire area covered by the footprints of the guide stars on the respective turbulent layer.

Figure 9 shows images of the PSF at various distances from the guide star. In single-star mode, the PSF shows significant elongation a few arcseconds away from the guide star. In GLAO operation this is dramatically better: the PSF remains circular up to a distance of 25″ from the guide stars. The elongation is caused by the different residual variance of the tilt in the direction toward and perpendicular to the guide star, as explained in, e.g., Hardy (1998).

We used the model described in § 3.1.1 to compare the measurements with theoretical expectations. Given the positions $\boldsymbol{\alpha}_i$ of the guide stars and the conjugation altitude h of the layer, we can numerically determine the corrected fraction $A_C(h,\boldsymbol{\alpha}_i)$ of the pupil footprint of the science object. Together with the temporal, fitting, and reconstruction errors, whose sum $\sigma^2_{\rm cl}$ can be retrieved from the on-axis performance, the total wave front error $\sigma^2_{\rm sci}$ for the science object is calculated with equation (3). Finally, the theoretical value for the FHWM can be calculated from $\sigma^2_{\rm sci}$ with equations (1) and (2), resulting in the curves plotted in Figure 8. The offset in the FHWM for the GLAO mode for the high-layer phase screen can be explained with the layer filter functions. For such a nonconjugated layer, the high spatial frequencies are not seen by the WFS and thus cannot be corrected, resulting in reduced overall performance.

This simple model describes the measurements very well. It only fails very close to the guide star, because it does not take into account diffraction and thus predicts an infinitely small FWHM at the position of the guide star. For a more accurate model in this regime, where $r_0 \sim D_{\rm tel}$, the telescope diameter $D_{\rm tel}$ must be included in the calculation of the FWHM with equation (2). Furthermore, this model does not take into account the spatial correlation of the Zernike modes and thus predicts a circularly symmetric PSF. Nevertheless, for the purpose of this work, this simple model has sufficient accuracy.

The integrated effect of multiple turbulent layers can be calculated by combining the results obtained in this section and in § 3.1. For single-star AO, the off-axis performance can be calculated as shown in § 3.1.1 and by adding the determined residual wave front variances $\sigma^2_{{\rm sci},i}(h,\alpha)$ of the individual layers

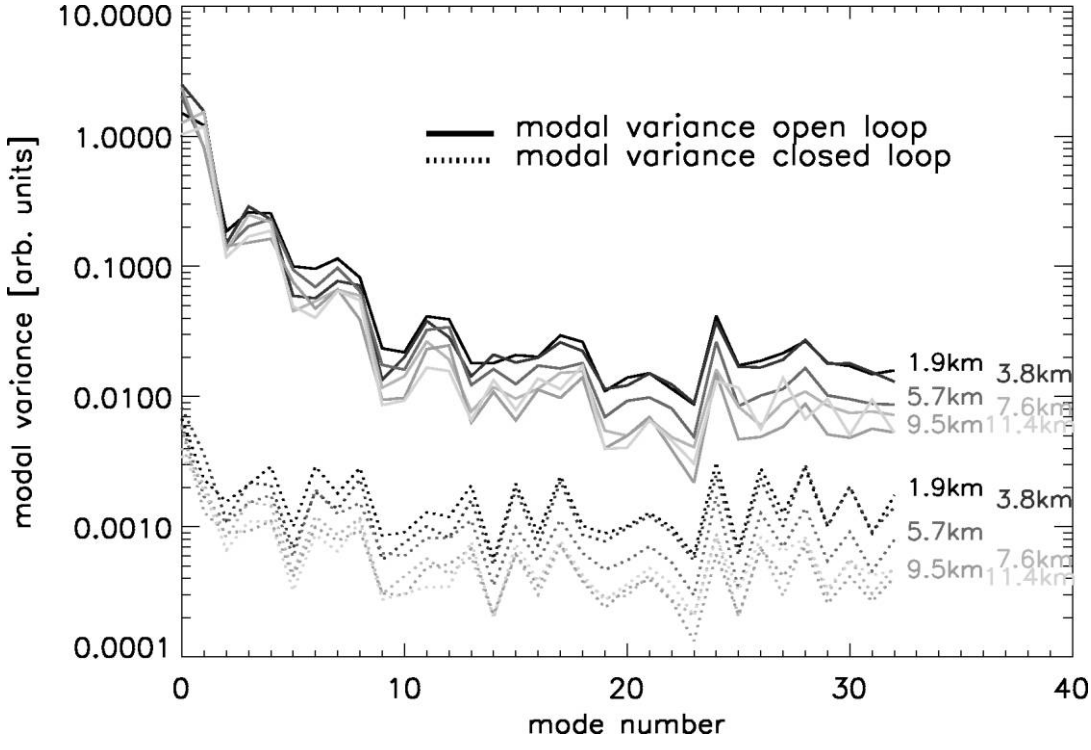

FIG. 7.—Measured temporal average variance of the modal coefficients in open loop and closed loop as a function of the distance between the phase screen and the conjugation height of the WFS, measured in GLAO mode. These measurements were conducted with a phase screen, which produces an equivalent seeing of 0.50″ at the wavelength used. [*See the electronic edition of PASP for a color version of this figure.*]

i at an altitude h and an off-axis angle of α. For GLAO mode, the FWHM of the off-axis PSF can be calculated similarly. However, one has to take into account that high-altitude layers are only partially corrected, according to the layer filter function described in § 3.1 and shown in Figures 4 and 6. Therefore, $\sigma^2_{\rm cl}$ in equation (3) has to be divided by the value of the layer filter function for the altitude of this layer. Furthermore, the corrected area $A_C(h,\alpha)$ used in the calculation of $\sigma^2_{{\rm sci},i}(h,\alpha)$ in equation (3) has to be modified according to the overlap with the footprints of all the guide stars on the considered layer. From the sum of $\sigma^2_{{\rm sci},i}(h,\alpha)$ for all the individual layers i, the total variance of the wave front can be determined and thus the off-axis FWHM.

3.4. Differential Brightness of the Guide Stars

One requirement of a layer-oriented MCAO system with optical co-addition is that all guide stars must have similar brightness. Otherwise, the measurements of the wave front aberrations have more weight in the direction of the brightest guide star, biasing the reconstruction process toward its position and yielding a nonuniform distribution of the performance in the FOV.

To experimentally investigate this effect, one phase screen with a conjugated altitude of 6.6 km above the telescope and four guide stars were used. The brightness of one guide star was gradually reduced with the help of a variable neutral density filter. The measured performance is plotted in Figure 10, showing a significant drop when the one guide star is only 0.25 mag fainter. If this guide star is more than ~1.5 mag fainter than the other three guide stars, it has practically no influence on the achievable performance. This confirms results obtained with end-to-end simulations of layer-oriented MCAO systems (Marchetti et al. 2003; Arcidiacono 2004).

For a real system, the value of the Strehl ratio in the field depends critically on the position and brightness of the guide stars and can be evaluated only through numerical simulations (see, e.g., Arcidiacono 2004; Nicolle et al. 2004; Tokovinin 2004); a simple semianalytical estimate is generally not possible. Nevertheless, a rough estimate can be derived for the simple case presented here, with only one turbulent layer.

The usual assumption is that the best correction of the wave front in the FOV is achieved at the position of the barycenter $\boldsymbol{p}_{\rm phot}$ of photons from all guide stars. In the case that all stars have the same brightness, this barycenter $\boldsymbol{p}_{\rm hom}$ coincides with the geometrical center $\boldsymbol{x}_{\rm stars}$ of the guide star distribution. In contrast, when the stars have different brightness, the barycenter of the inhomogeneous distribution $\boldsymbol{p}_{\rm inhom}$ is shifted, which in turn shifts the point of optimal correction away from $\boldsymbol{x}_{\rm stars}$. For a fixed science object located at $\boldsymbol{x}_{\rm stars}$, as for this system, the correction performance therefore apparently degrades. To

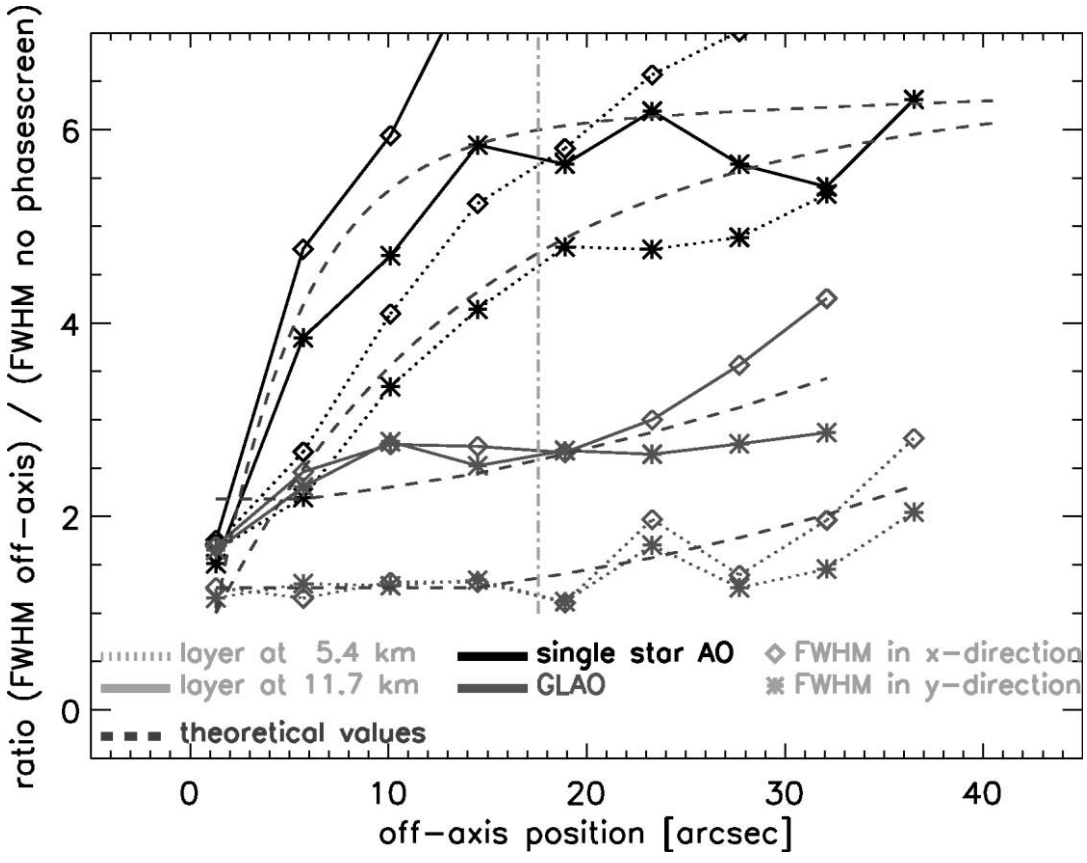

FIG. 8.—FWHM of the PSF of the science object as a function of the distance to the guide star for single-star AO and GLAO mode and for two different heights of the turbulent layer above the pupil plane. Three guide stars were used in GLAO mode, and the distance is given as the angular separation from one guide star. The position along the *x*-axis of the two other guide stars is indicated by the vertical dashed line. [*See the electronic edition of PASP for a color version of this figure.*]

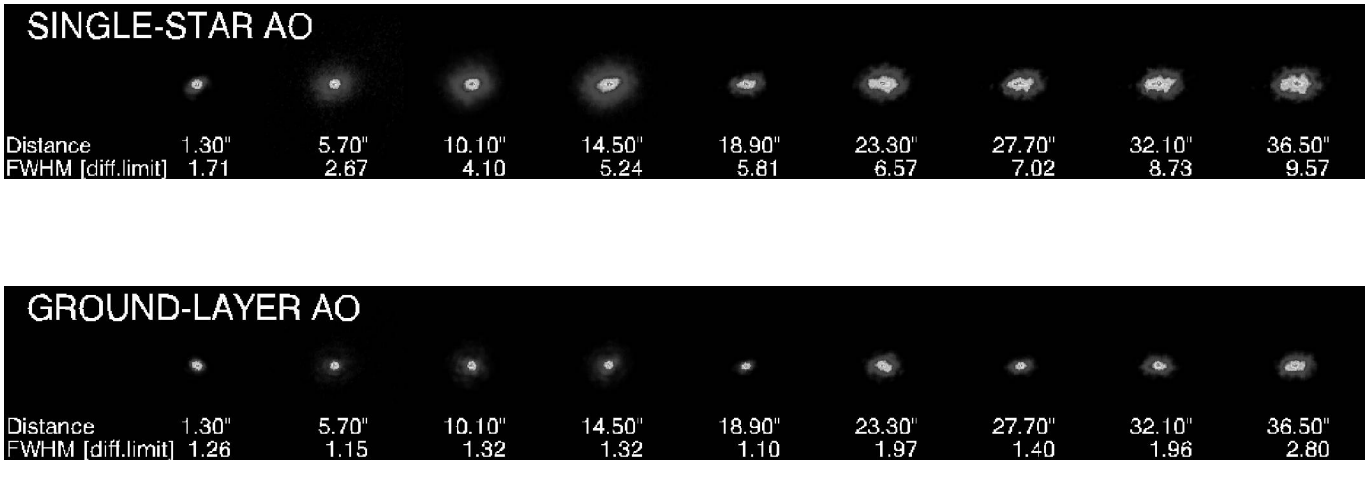

FIG. 9.—Images of the PSF of the science object as a function of the distance to the guide star for single-star AO (*top*) and GLAO (*bottom*) operation mode for one turbulent layer at 5.4 km above the pupil plane. The PSFs have been normalized to the same maximum intensity. The indicated FWHM is measured along the *x*-axis and is given in units of the diffraction limit. For comparison, the open loop FWHM is ~6.5 times the diffraction limit. [*See the electronic edition of PASP for a color version of this figure.*]

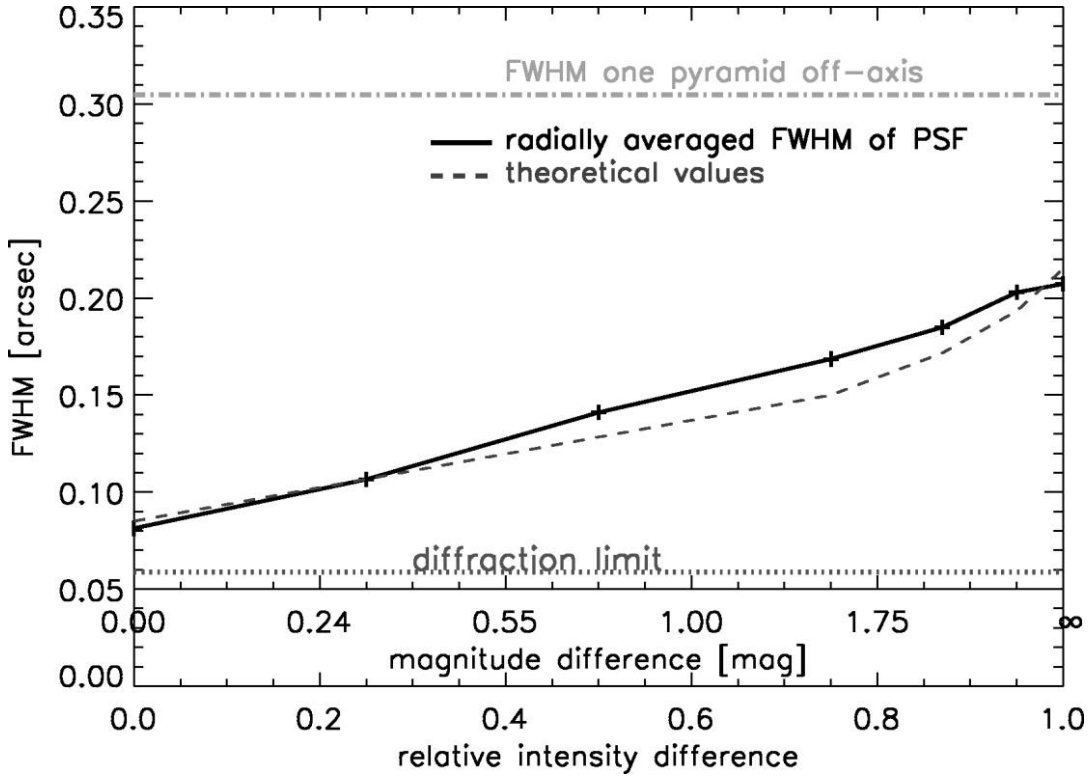

FIG. 10.—Measured FWHM of the PSF in GLAO operation mode as a function of the difference in the brightness of the guide stars. The brightness of three guide stars was matched and kept constant, while the fourth one was dimmed in discrete steps. [*See the electronic edition of PASP for a color version of this figure.*]

estimate the FHWM of this fixed science object, we reverse the situation and assume equal brightness of all guide stars, but the science object is shifted away from $\boldsymbol{x}_{\text{stars}}$ by the distance $|\boldsymbol{p}_{\text{hom}} - \boldsymbol{p}_{\text{inhom}}|$. Using the formalism described in the previous section for calculating the off-axis performance, the FWHM can be estimated. As shown in Figure 10, this simple model fits reasonably well with the measured data.

For brightness differences of more than ~1 mag, the model predicts a better performance than measured experimentally. The reason is that the CCD has a readout noise (RON) and a limited dynamic range, which are not considered in the analytical model. The signal of the fainter star is therefore either lost in the RON or results in homogenous illuminated pupil images. In either case, the faint star does not provide additional information about the wave front aberrations to improve the performance.

A different concept for an MCAO system is to measure the wave front aberrations in the direction of the single guide stars, just as in a classical AO system. By combining the information from the single guide stars numerically, the vertical structure of the turbulence can be retrieved and the appropriate commands for controlling the DM determined. One advantage of this concept is that with the help of sophisticated wave front reconstruction algorithms, optimal performance in the direction of the science object can be achieved (Petit et al. 2006). On the downside, this method requires rather bright guide stars, each of which has be to bright enough to serve as a guide star on its own. In contrast, in the layer-oriented method, as used in this paper, the light of all the guide stars is added up on one WFS CCD. In this case the individual guide stars can be faint: the important quantity is the total amount of the combined light from all guide stars. Since fainter stars are more abundant than brighter ones, the sky coverage of such systems is significantly increased as compared to classical AO, not only because of the increased field of correction but also because of the larger number of suitable guide stars (Arcidiacono 2004).

In the case of relatively few but bright guide stars of unequal magnitude, the star-oriented method is thus superior in performance to the layer-oriented method. On the other hand, the layer-oriented method can achieve a higher sky coverage because it can use fainter guide stars. A more detailed comparison based on extensive simulations of the achievable performance of the layer-oriented and the star-oriented approaches can be found in Bello et al. (2003a, 2003b).

4. CONCLUSION AND OUTLOOK

In this paper, we presented the first results obtained with a ground-layer adaptive optics (GLAO) experiment in the laboratory. A complete test bed for a GLAO system was set up,

and dynamic measurements using four natural guide stars, in layer-oriented operation mode with optical co-addition, were performed. For the first time, these concepts were successfully verified in dynamic operation.

The performance of this system in GLAO mode was extensively characterized in closed loop. It was shown that the concept of layer-oriented GLAO with optical co-addition works, with results very similar to those predicted by numerical simulations. The filtering of nonconjugated turbulent layers matches very well with semianalytical expectations based on layer filter functions. Moreover, the shape of the PSF in the field follows the predictions. The PSF is uniform over the entire field, covered by guide stars, leading to an increase in the area with useful correction by a factor of ~25 in this system as compared to single-star AO.

In addition, the impact of differences in the brightness of the individual guide stars on the correction efficiency was studied. A star that is more than ~1.5 mag fainter than the others was found to have no influence on the performance of the system.

The work was funded by the Alexander von Humboldt Foundation through the Wolfgang Paul Prize. We are grateful to Florian Briegel, Frank Kittmann, and Udo Neumann for their help in developing the control software package, Peter Bizenberger for much advice on optical design, Felix Hormuth and Stefan Hippler for their support on the dynamic turbulence simulator (MAPS), and Lars Mohr and Karl Wagner for taking care of the electronics. Furthermore, we want to thank the whole team of the mechanical workshop at the MPIA, especially Ralf-Rainer Rohloff, Norbert Muench, Armin Boehm, and Wolfgang Sauer, for the design and manufacturing of all the required hardware components.

REFERENCES

Andersen, D., et al. 2006, PASP, 118, 1574
Arcidiacono, C. 2004, Ph.D. thesis, Univ. studi Firenze
Athey, A., Shectman, S., Schechter, P., & Lane, B. 2004, Proc. SPIE, 5490, 960
Avila, R., Masciadri, E., Vernin, J., & Sánchez, J. 2004, PASP, 116, 682
Babcock, H. W. 1953, PASP, 65, 229
Baranec, C., Lloyd-Hart, M., Codona, J., & Milton, N. 2003, Proc. SPIE, 5169, 341
Baranec, C., Lloyd-Hart, M., & Milton, N. M. 2007, ApJ, 661, 1332
Beckers, J. 1988, in ESO Conf., Very Large Telescopes and Their Instrumentation, ed. M.-H. Ulrich (Garching: ESO), 693
Bello, D., Conan, J.-M., Rousset, G., Tordi, M., Ragazzoni, R., Vernet-Viard, E., Kasper, M., & Hippler, S. 2003a, Proc. SPIE, 4839, 612
Bello, D., Verinaud, C., Conan, J.-M., Fusco, T., Carbillet, M., & Esposito, S. 2003b, Proc. SPIE, 4839, 554
Butler, D., Hippler, S., Egner, S., Xu, W., & Bär, J. 2004, Appl. Opt., 43, 2813
Costa, J. 2005, Appl. Opt., 44, 60
Diolaiti, E., Farinato, J., & Soci, R. 2005, Tech. Rep. LN-INAFA-FDR-AO-001 (Heidelberg: MPIA)
Egner, S., Masciadri, E., McKenna, D., Herbst, T. M., & Gaessler, W. 2006, Proc. SPIE, 6272, 627257
Egner, S., et al. 2004, Proc. SPIE, 5490, 924
Farinato, J., Ragazzoni, R., & Diolaiti, E. 2004a, Proc. SPIE, 5490, 1229
Farinato, J., et al. 2004b, Proc. SPIE, 5382, 578
Fried, D. 1965, J. Opt. Soc. Am., 55, 1427
Hardy, J. W. 1998, Adaptive Optics for Astronomical Telescopes (Oxford: Oxford Univ. Press), chap. 7.4
Hippler, S., Hormuth, F., Brandner, W., Butler, D., Henning, T., & Egner, S. 2006a, Proc. SPIE, 6272, 627255
Hippler, S., Hormuth, F., Butler, D., Brandner, W., & Henning, T. 2006b, Opt. Express, 14, 10139
Hubin, N., Louarn, M. L., Conzelmann, R., Delabre, B., Fedrigo, E., & Stuik, R. 2004, Proc. SPIE, 5490, 846
Jolissaint, L., Veran, J.-P., & Stoesz, J. 2004, Proc. SPIE, 5382, 468
Le Louarn, M., & Hubin, N. 2006, MNRAS, 365, 1324
Marchetti, E., Ragazzoni, R., & Diolaiti, E. 2003, Proc. SPIE, 4839, 566
Morris, T., Berry, P., Butterley, T., Clark, P., Dunlop, C., Myers, R., Saunter, C., & Wilson, R. 2004, Proc. SPIE, 5490, 891
Nicolle, M., Fusco, T., Michau, V., Rousset, G., Blanc, A., & Beuzit, J.-L. 2004, Proc. SPIE, 5490, 858
Noll, R. 1976, J. Opt. Soc. Am., 66, 207
Owner-Petersen, M., & Gontcharov, A. 2002, J. Opt. Soc. Am., 19, 537
Petit, C., Conan, J.-M., Kulcsar, C., Raynaud, H.-F., Fusco, T., Montri, J., & Rabaud, D. 2006, Proc. SPIE, 6272, 62721T
Prieur, J.-L., Daigne, G., & Avila, R. 2001, A&A, 371, 366
Racine, R., & Ellerbroek, B. 1995, Proc. SPIE, 2534, 248
Ragazzoni, R. 1996, J. Mod. Opt., 43, 289
Ragazzoni, R., Diolaiti, E., Farinato, J., Vernet, E., Baruffolo, A., Crimi, G., Tommelleri, R., & Rossettini, F. 2002, Tech. Rep. OWL-TRE-INA-60000-0036 (Arcetri: INAF)
Ragazzoni, R., Diolaiti, E., Vernet, E., Farinato, J., Marchetti, E., & Arcidiacono, C. 2005, PASP, 117, 860
Ragazzoni, R., Farinato, J., & Marchetti, E. 2000, Proc. SPIE, 4007, 1076
Rigaut, F. 2002, in Proc. Beyond Conventional Adaptive Optics, ed. E. Vernet et al. (Garching: ESO), 11
Rigaut, F., Ellerbroek, B., & Flicker, R. 2000, Proc. SPIE, 4007, 1022
Stuik, R., Hippler, S., Feldt, M., Aceituno, J., & Egner, S. 2004, Proc. SPIE, 5490, 1572
Tokovinin, A. 2004, PASP, 116, 941
Tokovinin, A., Louarn, M. L., & Sarazin, M. 2000, J. Opt. Soc. Am. A, 17, 1819
Tokovinin, A., Thomas, S., Gregory, B., van der Bliek, N., Schurter, P., Cantarutti, R., & Mondaca, E. 2004, Proc. SPIE, 5490, 870